Wolf-Rayet Stars
W.-R. Hamann, A. Sander, H. Todt, eds.
Potsdam: Univ.-Verlag, 2015
URL: http://nbn-resolving.de/urn:nbn:de:kobv:517-opus4-84268

Eta Carinae: Many Advances .... Even More Puzzles

T. R. Gull[1]
[1] *Code 667, NASA/GSFC, Greenbelt, MD, USA*

Since Augusto Damineli's demonstration in 1996 that Eta Carinae is a binary with a 5.52 year period, many innovative observations and increasingly advanced three-dimensional models have led to considerable insight on this massive system that ejected at least ten, possibly forty, solar masses in the nineteenth century. Here we present a review of our current understanding of this complex system and point out continuing puzzles.

1 The Historical η Car

Eta Argus (η Car in earlier nomenclature) burst upon the astronomical scene in the 1840s when southern observers noted the star brightened to rival Sirius, then faded (Davidson & Humphreys 1997). Late in the nineteenth century, it again brightened to almost naked-eye visibility, then faded. By the 1940s, Gaviola (1950, 1953) noted that the star was again brightening. Gaposchkin (1954) suggested η Car as a galactic nova with a possible period of 16.5 years. Later Zanella et al. (1984) noticed a potential eleven year period. Neugebauer & Westphal (1968) noted that η Car was the brightest ten micron source outside of the solar system. Davidson et al. (1986) noted that spectra, recorded of associated nebular ejecta by the *International Ultraviolet Explorer* and facilities at Cerro Tololo Inter-American Observatory, showed greatly enhanced nitrogen at the expense of carbon and oxygen, signifying that the Great Eruption of the 1840s came from a very massive star. Yet a stellar remnant with $5{\times}10^6$ $L_\odot$, remained. Weigelt & Ebersberger (1986), using ground-based speckle interferometry, noted that four point-like sources, separated by less that 0.3", were present. Even with the uncorrected primary optics of the Hubble Space Telescope, Weigelt et al. (1995) confirmed the four point-like structures using the Faint Object Camera (see Figure 1, Left), but Davidson et al. (1995), with the Faint Object Spectrograph, determined that the brighter component was a point stellar source, but the other three sources, commonly known as Weigelt blobs B, C and D, were very bright nebular clumps rivaling the brightness of the ionizing source.

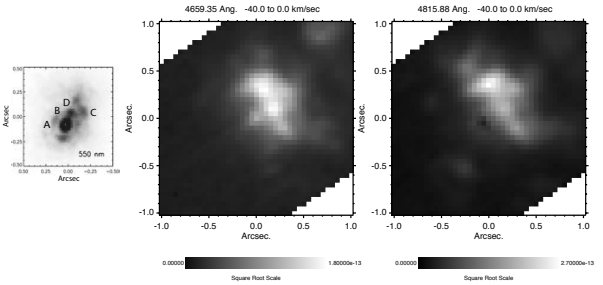

Fig. 1: The central region about η Car as imaged with HST. Left: FOC deconvolved imagery with the 550M filter, recorded in 1992 (Weigelt et al. 1995). Middle: STIS [Fe III] 4659Å and Right: STIS [Fe II] 4815Å. The continuum-subtracted STIS images, recorded in 2012, are 40 km/s wide centered at -20 km/s (Gull et al. in prep). In the two decades between the FOC and STIS observations, the central source brightened at least five-fold and the emission sources expanded and changed. Note that the forbidden emission line structures are exterior to the stellar point source.

2 What we learned since 1996

2.1 η Car has a 5.5-year period!

Interest greatly increased with the discovery by Damineli (1996) that η Car had a 5.52-year period defined by the drop in ionization state associable with the periastron passage, that was traceable back to the 1940s through spectroscopy by Gaviola (1950) and others. Corcoran et al. (1997) demonstrated that variable X-ray emission was associable with the interacting winds of η Car and began monitoring the X-ray flux with the Rossi X-ray Timing Explorer (*RXTE*). Steiner & Damineli (2004) detected He II 4686Å and its strengthening leading up to disappearance across the low (periastron) state. Ground-based spectroscopy and X-ray photometry has continued through early 2015 with focus on the behavior of He II 4686Å and X-ray flux especially across the periastron events (Damineli et al. 2008; Teodoro et al. 2012). The most current period measures are from X-ray photometry: 2023.7+/- 0.7 days (Corcoran et al., submitted; see Corcoran, these proceedings), and from He II 4686Å: 2022.7+/-0.8 days (Teodoro et al., submitted).

Crucial to the studies of η Car over the past two decades has been the *HST* with the Wide Field/Planetary Camera-2 (WFPC2) (Trauger et al. 1994) and the Space Telescope Imaging Spectrograph (STIS) (Kimble et al. 1998), both of which optimally sampled at, or close to, the diffraction limit of the *HST*.

The *HST*/WFPC2 provided sharp imagery of the Homunculus (see Middle of Figure 2) that revealed the dusty structure appeared to be bipolar with an

intervening skirt. Repeated visits revealed expansion over the sixteen year lifetime of WFPC2 in HST and the changing structure in the NUV within the Homunculus to the northwest (Smith et al. 2004). From early 1998 to 2004, a series of observations with the STIS recorded spectra of the star and selected emission structures within the Homunculus from below Lyman α to one micron. Hillier et al. (2001, 2006) using *CMFGEN* (Hillier & Miller 1998) to match the UV spectrum, found no direct evidence for η Car B, the secondary star, largely because of the very dense, extended wind of η Car A. While the spectrum of η Car B should peak in the Far UV, accessible to the Far Ultraviolet Spectrographic Explorer, *FUSE*, signatures of the primary wind and intervening material completely swamps any direct evidence.

Indirect evidence for the secondary star arises from X-ray spectroscopy. Pittard & Corcoran (2002) generated synthetic X-ray spectra that required a secondary mass loss rate, $\dot{M}_{\rm b} \approx 10^{-5}\ M_{\odot}{\rm yr}^{-1}$ with $v_{b,t} \approx 3000\ {\rm km\,s^{-1}}$. More recent models support those values for η Car B with the estimated values of $\dot{M}_{\rm a} \approx\ 8.5{\times}10^{-4}\ {\rm yr}^{-1}$ with $v_{a,t}$ =420 ${\rm km\,s^{-1}}$ (Madura et al. 2013, see also T. Madura, these proceedings).

Ground-based spectroscopy of η Car is greatly contaminated by both emission and scattered star light from associated nebulosities. Indeed approximately half of the visible radiation comes from the Homunculus and structures within. An extreme example is presented in Figure 1 which compares the emission recorded through the FOS 550M filter to low velocity images from the STIS centered on [Fe III] 4659.35Å and [Fe II] 4815.88Å. Within the central 0.15" region centered on η Car no [Fe II] and little [Fe III] emission is present. Teodoro et al (submitted) demonstrated that He II 4686Å originates in this central core and that ground-based measures overestimate core continuum due to starlight scattered by nearby structures. Hence, spatially-resolved spectroscopy with *HST*/STIS is critical for in-depth understanding of the central source AND the surrounding nebular structures.

2.2 The associated nebular structures

η Car is exceptional because 1) it has gone through major ejections within historical times, 2) the 1840s huge mass ejection kinetically rivals a supernova event but a massive binary survived, and 3) the massive binary has such massive interacting winds that many forbidden emission lines, characteristic of relatively high densities ($n_e \approx 10^7\,{\rm cm^{-3}}$) and relatively low ionization (I<40 eV and, for many structures, I<13.6 eV). Much can be learned about the ejecting star, the expanding ejecta – how the massive amounts of material evolve from heated, dense stellar atmospheres to compressed, rapidly cooling shells of gas that rapidly lead to molecular and dust formation – and the ongoing winds that form detectable fossil structures. Even more can be learned about nebular structures as a wide range of photoionization, temperature, density, shocks exists in the interacting winds, their persisting fossil structures, neutral- , ionized metal- and H II-regions, We can examine the multi-tiered structures that are spatially resolved by *HST*, spectrally probed by *Herschel* and many ground-based telescopes, especially instruments on the multiple *VLT* telescopes.

2.2.1 The Homunculus

Gaviola (1950) coined the name, Homunculus, based upon the humanoid-apparent nebulosity he photographed in the 1940s. As shown in Figure 2 (Middle), the *HST* visible wavelength image reveals a dusty, bipolar shell, centered on η Car with an apparent skirt located between the two lobes.

Spatially-resolved long slit spectra from Davidson et al. (2001) used a single *HST*/STIS long slit spectrum across the central axis and the *HST*/WFPC2 imagery to demonstrate the hourglass shape of the Homunculus. Five Gemini long-slit spectra in the near infrared detected a thin shell of H_2 that bounds a thicker interior structure seen in NIR [Fe II] (Smith 2006). A minimum of 10 $M_{\odot}$ of H_2 was estimated based upon an average density of 10^6 ${\rm cm^{-3}}$. However, Gull et al. (2005) derived densities of $n_e \approx 10^7$ ${\rm cm^{-3}}$ in a thin, interior, low-ionization, absorbing shell at a radial velocity of -513 km ${\rm s^{-1}}$.

More recently, *VLT*/XShooter mapping of the H_2 (Steffen et al. 2014, see Figure 2) demonstrated that the bipolar geometry is distorted by (1) holes in the caps near the axis of symmetry, (2) grooves in the caps that are point-symmetrical relative to the central source, (3) two proturbences near the equatorial region that roughly correspond to the 120^o angular separation of the bowshock defined by the interacting binary winds (see Subsection 2.2.5) and (4) significant dust between the fore and back walls, or interior to the H_2 shell.

The *HST*/STIS provided very high-spectral, high-spatial resolution spectroscopy from 1175 to 3160Å at critical orbital phases in the early 2000s from apastron across the 2003.5 periastron event (Gull et al. 2005; Nielsen et al. 2005). At an expansion velocity of -513 km ${\rm s^{-1}}$, nearly a thousand H_2 absorption lines were identified in the FUV as well as a similar number of singly-ionized metals absorption lines, including first time detection of V^+, Sr^+ and Sc^+ in interstellar space. Additionally, absorptions from CH, OH, CH^+ and NH in the NUV were seen originating from the ground state ($T_{\rm e} < 40\,{\rm K}$)(Verner et al. 2005b), but ionic metals at -513 km ${\rm s^{-1}}$ show transitions originating from energy levels consistent with $T_{\rm e} = 760\,{\rm K}$. While the many H_2 absorption lines were present across the broad high state, they

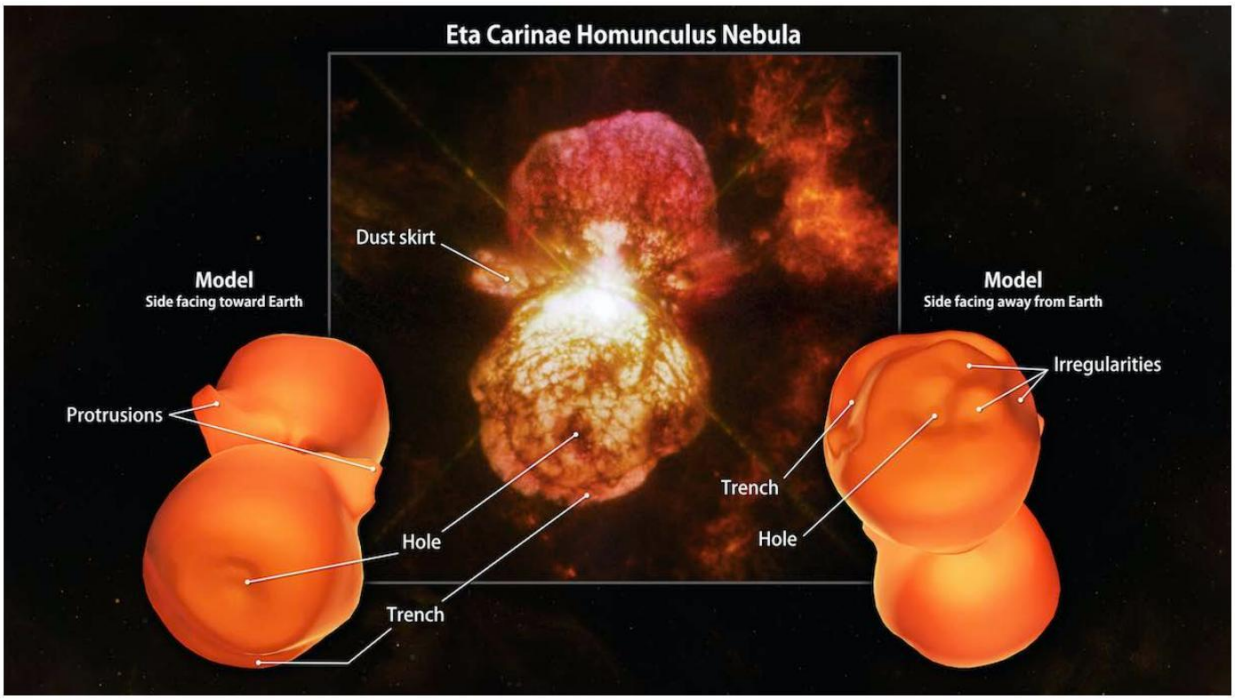

Fig. 2: Comparison of H_2 to the light-scattering dust spatial structures. Left: Projection of H_2 as seen from Earth. Center: *HST/WFPC2* image in near red light. Right: Projection of H_2 as seen from far side. Both the H_2 and dust images show evidence for side trenches and holes near center of the lobe caps, the dusty skirt is not seen in H_2, but two protrusions appear to correlate with obscurations against the far lobe. Likely the H_2 has been destroyed by ultraviolet radiation in the skirt region and interior to the thin H_2 shell.

disappear during the low ionization state as UV radiation short ward of 1700 Å disappears within the Homunculus across periastron. Additionally, absorption systems with velocities ranging between -513 and -384 km s^{-1} are present with with column densities that decrease with decreasing velocities. Is this evidence of changing mass loss properties between the 1840s and 1890s eruptions?

Despite η Car being the brightest ten-micron source (Neugebauer & Westphal 1968), the total amount of material ejected continues to be poorly determined. Chesneau et al. (2005) found the warm dust in the central 3" is corundum (Al_2O_3) and silicates. However, cooler dust and molecules exist in the outer Homunculus and are not easily quantified without additional studies and dust modeling. Consistent with the lower limit placed by Smith (2006), Morris (these proceedings) estimates that the total ejecta could exceed 40 $M_\odot$!

2.2.2 The Little Homunculus

Detailed mapping of the Homunculus with the *HST*/STIS 52" $\times$ 0.1" aperture, led to the detection of an ionized, internal bipolar structure, the Little Homunculus, seen in a number of [Fe II] lines with characteristic critical densities of $N_e = 10^6\,cm^{-3}$. The Little Homunculus has a line of sight at -147 km s^{-1}, but its caps expand at 300 km s^{-1}. Ishibashi et al. (2003) estimated a total mass of 0.1 to 0.5 $M_\odot$. STIS-measured proper motions are consistent with the 1890s mass ejection. While not seen during the high ionization state, saturated Ti^+ (ionization potential 13.58 eV) absorptions appear during the several month long low ionization state, signifying brief disappearance of Lyman continuum photons during periastron passage (Gull et al. 2006).

2.2.3 The Strontium Filament and the Butterfly

A most curious set of emission lines were noticed in the STIS spectra redward of Hα located about 2" north of η Car. Zethson et al. (2001) identified them to be [Sr II], leading to labeling this structure, the Strontium Filament. Hartman et al. (2004) found hundreds of forbidden emissions from singly-ionized metals with most being [Ti II]. These spectra led to greatly improved atomic models of singly-ionized iron-peak elements including Ti^+, Ni^+, Sc^+, Cr^+ and Mn^+ and reinforcement that both carbon and oxygen are so depleted that normal molecular and dust formation involving these elements is greatly reduced i.e. the chemistry leading to dust formed in the ejecta of η Car is very peculiar (Bautista et al.

2006, 2009, 2011).

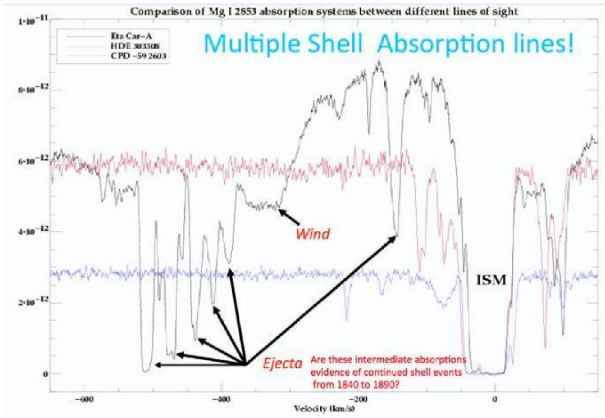

Fig. 3: Intermediate velocities seen in line of sight Multiple absorption components are seen in low ionization systems between -513 and -384 km s^{-1}. Are these evidence of declining wind properties between the 1840s and 1890s ejections?

Chesneau et al. (2005) noted that in the NIR a several arcsecond-sized butterfly-shaped cavity surrounds η Car. A spot inspection of these structures using STIS mapping spectra, discussed in section 2.2.5, indicate the butterfly boundaries are fainter versions of the Strontium Filament.

2.2.4 The Weigelt Blobs

The three very bright point-like emission structures, called Weigelt B, C and D (Weigelt & Ebersberger 1986), provide major clues as to the properties of the η Car binary and its recent history. Zethson et al. (2012) did a complete spectral inventory of Weigelt B and D from 1700 to 10,000Å during the low- and high-ionization states. Differences in nebular photoionization between the low- and high-ionization states led to estimates of the FUV properties of the secondary (Verner et al. 2005a; Mehner et al. 2010). With a temperature range from 32,000 to 39,000 K and $4{\times}10^5$ to 10^6 $L_\odot$, and mass loss rates estimated to be $\dot{M}{\approx}10^{-5}$ $M_\odot$yr^{-1}, the hidden secondary could still be an early WN or O star. Teodoro et al. (submitted) find that the blobs are partially-ionized surfaces of large, slow moving ejecta, possibly thrown out in the 1890s event. More observations and modeling are needed.

2.2.5 The Fossil Winds

The *HST*/STIS long slit observations indicated considerable wind/nebular emission structures in addition to the central binary and the Weigelt blobs and led to systematic mapping of the central 2"×2" region from June 2009 to March 2015, which spans the 5.53-year binary cycle (Gull et al., in prep). Spatially-resolved velocity structures extend out to 0.7" and from -420 to +400 km s^{-1} in multiple permitted and forbidden lines. Two forbidden lines, [Fe III] 4659Å and [Fe II] 4815Å, are well isolated and prove to be very effective tracers of fossil wind structures ranging from those being formed in the current cycle and those formed in previous cycles 5.52, 11.04, 16.08 years previously. To date, η Car uniquely provides these fossil winds because of the very massive interacting winds, highly eccentric orbit and hence variable ionization states. These forbidden emissions have critical densities, $N_e = 10^7$ cm^{-3} that are obtained by the interacting winds and resulting shocks.

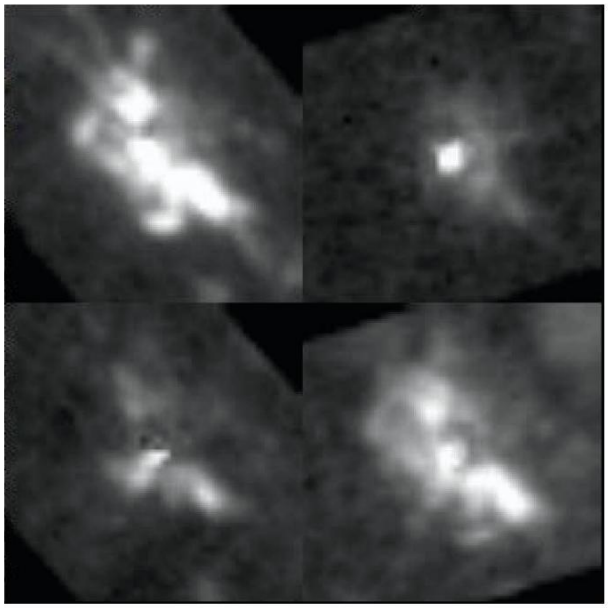

Fig. 4: Changes in photoionization of the fossil winds between the high- and low-ionization states Note the [Fe III] features at periastron (upper left) appear as [Fe II] features at apastron (lower right) correcting for 2.7 years expansion. Maps of continuum-subtracted [Fe III] 4659Å (upper row) and [Fe II] 4815Å (lower row) at apastron (left column) and periastron(right column). Field of view is 2". Velocity interval is -160 to -120 km s^{-1}.

Teodoro et al. (2013), using several sets of maps of [Fe II] and [Ni II] emissions recorded across the broad high state from 2010 to 2013, demonstrated that the red-shifted shells of primary wind were expanding at 470 km s^{-1}, consistent with the modeled primary wind velocity, 420 km s^{-1} as determined by Groh et al. (2012). These studies reinforce the three dimensional modeling of the interacting winds (Gull et al. 2009, 2011; Madura 2011; Madura et al. 2013, and Madura, this volume).

3 Questions that continue to challenge us today:

Our vantage point is such that several stellar magnitudes obscure our view. Yet so much nebular structure is in the vicinity that we can obtain indirect measures of the massive binary and answer some of our questions. However, for each question that is answered, two more questions appear. These include:

What is the current secondary?

Which star ejected during the Great Eruption?

Was the event a merger?

What caused the H_2 protrusions and are they clues to the ejection mechanism?

Are the multiple absorption velocities between -512 and -384 km/s evidence for decreasing primary mass loss properties between the 1840s and the 1890s events?

How and where did (do) molecules and dust form?

What is the total mass ejected in the Great Eruption?

How stable is the current binary system?

When will a supernova occur?

As I move to emeritus status at Goddard, I most sincerely thank the many collaborators with whom I have enjoyed these studies these past two decades.

References

Bautista, M. A., Ballance, C., Gull, T. R., et al. 2009, MNRAS, 393, 1503

Bautista, M. A., Hartman, H., Gull, T. R., Smith, N., & Lodders, K. 2006, MNRAS, 370, 1991

Bautista, M. A., Meléndez, M., Hartman, H., Gull, T. R., & Lodders, K. 2011, MNRAS, 410, 2643

Chesneau, O., Min, M., Herbst, T., et al. 2005, A&A, 435, 1043

Corcoran, M. F., Ishibashi, K., Davidson, K., et al. 1997, Nature, 390, 587

Damineli, A. 1996, ApJ, 460, L49

Damineli, A., Hillier, D. J., Corcoran, M. F., et al. 2008, MNRAS, 384, 1649

Davidson, K., Dufour, R. J., Walborn, N. R., & Gull, T. R. 1986, ApJ, 305, 867

Davidson, K., Ebbets, D., Weigelt, G., et al. 1995, AJ, 109, 1784

Davidson, K. & Humphreys, R. M. 1997, ARA&A, 35, 1

Davidson, K., Smith, N., Gull, T. R., Ishibashi, K., & Hillier, D. J. 2001, AJ, 121, 1569

Gaposchkin, C. P. 1954, Variable Stars & Galactic Structure. (Athlone Press)

Gaviola, E. 1950, ApJ, 111, 408

Gaviola, E. 1953, ApJ, 118, 234

Groh, J. H., Hillier, D. J., Madura, T. I., & Weigelt, G. 2012, MNRAS, 423, 1623

Gull, T. R., Kober, G. V., & Nielsen, K. E. 2006, ApJS, 163, 173

Gull, T. R., Madura, T. I., Groh, J. H., & Corcoran, M. F. 2011, ApJ, 743, L3

Gull, T. R., Nielsen, K. E., Corcoran, M. F., et al. 2009, MNRAS, 396, 1308

Gull, T. R., Vieira, G., Bruhweiler, F., et al. 2005, ApJ, 620, 442

Hartman, H., Gull, T., Johansson, S., Smith, N., & HST Eta Carinae Treasury Project Team. 2004, A&A, 419, 215

Hillier, D. J., Davidson, K., Ishibashi, K., & Gull, T. 2001, ApJ, 553, 837

Hillier, D. J., Gull, T., Nielsen, K., et al. 2006, ApJ, 642, 1098

Hillier, D. J. & Miller, D. L. 1998, ApJ, 496, 407

Ishibashi, K., Gull, T. R., Davidson, K., et al. 2003, AJ, 125, 3222

Kimble, R. A., Woodgate, B. E., Bowers, C. W., et al. 1998, ApJ, 492, L83

Madura, T. I., Gull, T. R., Okazaki, A. T., et al. 2013, MNRAS, 436, 3820

Madura, T. I. e. a. 2011, MNRAS, 125, 102

Mehner, A., Davidson, K., Ferland, G. J., & Humphreys, R. M. 2010, ApJ, 710, 729

Neugebauer, G. & Westphal, J. A. 1968, ApJ, 152, L89

Nielsen, K. E., Gull, T. R., & Vieira Kober, G. 2005, ApJS, 157, 138

Pittard, J. M. & Corcoran, M. F. 2002, A&A, 383, 636

Smith, N. 2006, ApJ, 644, 1151

Smith, N., Morse, J. A., Collins, N. R., & Gull, T. R. 2004, ApJ, 610, L105

Steffen, W., Teodoro, M., Madura, T. I., et al. 2014, MNRAS, 442, 3316

Steiner, J. E. & Damineli, A. 2004, ApJ, 612, L133

Teodoro, M., Damineli, A., Arias, J. I., et al. 2012, ApJ, 746, 73

Teodoro, M., Madura, T. I., Gull, T. R., Corcoran, M. F., & Hamaguchi, K. 2013, ApJ, 773, L16

Trauger, J. T., Ballester, G. E., Burrows, C. J., et al. 1994, ApJ, 435, L3

Verner, E., Bruhweiler, F., & Gull, T. 2005a, ApJ, 624, 973

Verner, E., Bruhweiler, F., Nielsen, K. E., et al. 2005b, ApJ, 629, 1034

Weigelt, G., Albrecht, R., Barbieri, C., et al. 1995, in Revista Mexicana de Astronomia y Astrofisica Conference Series, Vol. 2, Revista Mexicana de Astronomia y Astrofisica Conference Series, ed. V. Niemela, N. Morrell, & A. Feinstein, 11

Weigelt, G. & Ebersberger, J. 1986, A&A, 163, L5

Zanella, R., Wolf, B., & Stahl, O. 1984, A&A, 137, 79

Zethson, T., Gull, T. R., Hartman, H., et al. 2001, AJ, 122, 322

Zethson, T., Johansson, S., Hartman, H., & Gull, T. R. 2012, A&A, 540, A133

André-Nicolas Chené: Is there any remaining argument to support the idea that η Car is *not* a binary?

Ted Gull: The recent periastron event (August 2014) arrived on schedule. Both X-ray and He II 4686Å photometry are consistent with binarity. But there will always be doubters.

Paul Crowther: Although η Car is unique it might resemble the nebula associated with AG Car in 10^4 years and NaSt1 (WR 122) shares some nebular similarities to η Car (high N/O ratio, high density, hot dust).

Ted Gull: The phase – post outburst – of η Car is transient. Likely the ejecta disperses on timescales of 10^4 years. There is no obvious evidence of another post outburst comparable to η Car in the Milky Way. But that does not exclude NaSt1 as being a more evolved analog.